Electronic Supplementary Material (ESI) for Journal of Materials Chemistry A.

Promoting Charge Transfer in Hyperbranched, Trisoctahedral-shaped Core-Shell Au@PdPt Nanoparticles by Facet-dependently Constructing Transition Pd Layer as High Performance Electrocatalysts

Yahui Song,[a] Cuixia Bi,[a] Chenshuo Wu,[a] Hongpeng He,[a] Lihui Huang,[b] Dayang Wang[c] and Haibing Xia[*,a]

[a] State Key Laboratory of Crystal Materials, Shandong University, Jinan, 250100, P. R. China

[b] School of Environmental Science and Engineering, Shandong University, Jinan, 250100, P. R. China;

[c]State Key Laboratory of Inorganic Synthesis and Preparative Chemistry, College of Chemistry, Jilin University, Changchun 130012, P. R. China

E-mail: hbxia@sdu.edu.cn

Figure S1. HRTEM images of nanobranches on HTCS $Au_{100}@Pd_{20}Pt_{20}$ NPs with defects (such as atomic steps, kinks, and corner atoms).

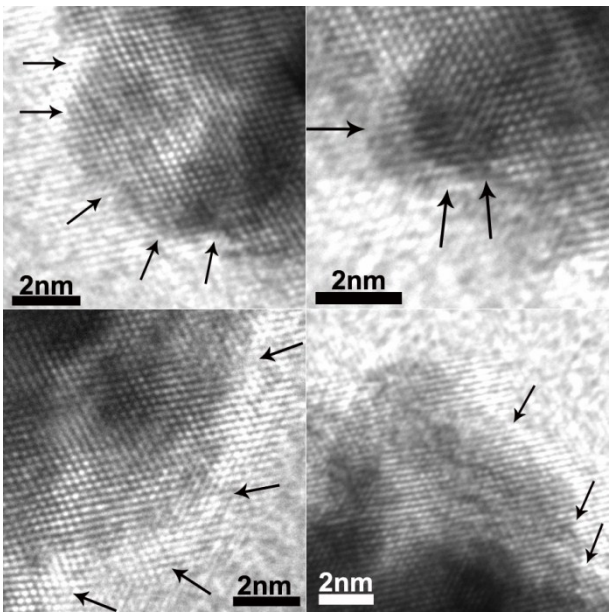

Figure S2. The digital photos of the aqueous solutions of TOH Au NPs (a), Au@Pd NPs prepared by only adding Pd^{2+} ions before the addition of second batch of AA solution (b), Au@Pd NPs prepared by adding both Pd^{2+} and Pt^{2+} ions before the addition of second batch of AA solution (c), and HTCS $Au_{100}@Pd_{20}Pt_{20}$ NPs (d), respectively.

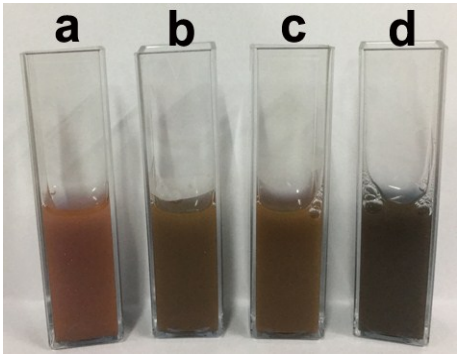

Figure S3. Low (a) and high magnification (b) TEM images of TOH-shaped Au@Pd NPs prepared by adding both Pd^{2+} and Pt^{2+} ions before the addition of second batch of AA solution, HRTEM images (c) recorded from the boxed area of (b), viewed along the ⟨011⟩ direction and HAADF-STEM-EDS cross-sectional compositional line profile (d) of one TOH-shaped Au@Pd NP, in which red and blue colors represent the elemental Au and Pd, respectively. The inset in (c) is the corresponding FFT image.

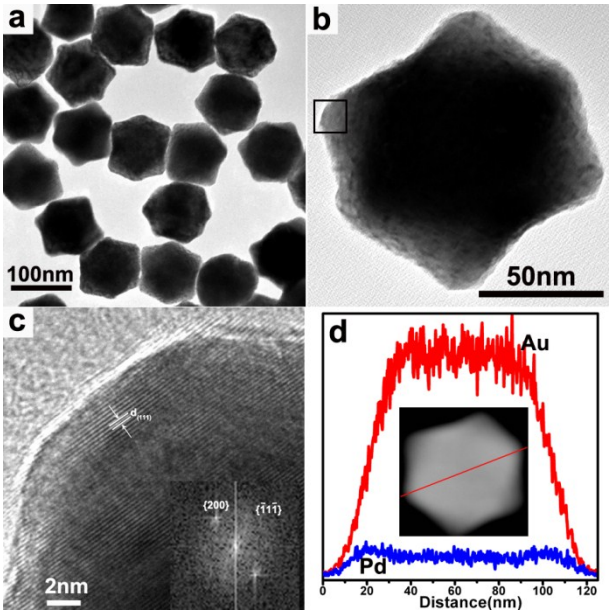

Figure S4. Low (a) and high magnification (b) TEM images of TOH-shaped Au@Pd NPs prepared by only adding Pd^{2+} ions before the addition of second batch of AA solution.

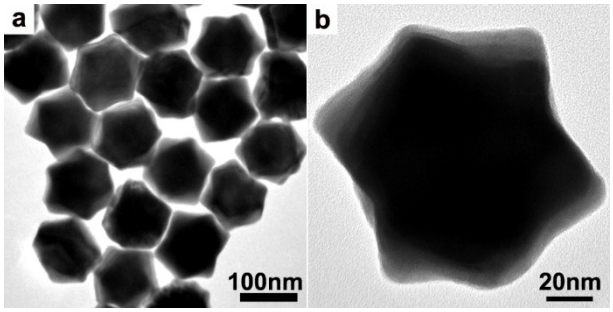

Figure S5. XRD pattern of as-prepared HTCS $Au_{100}@Pd_{20}Pt_{20}$ NPs.

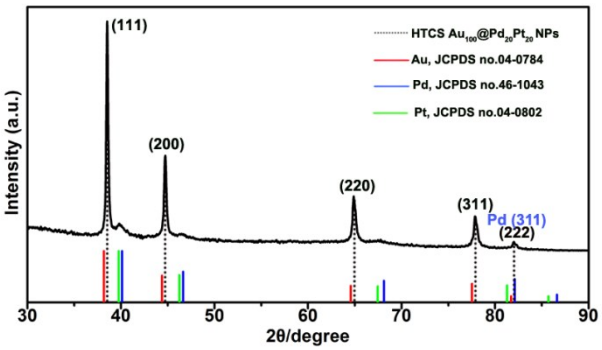

Figure S6. Low (a) and high magnification (b) TEM image of CS $Au_{100}@Pt_{20}$ NPs.

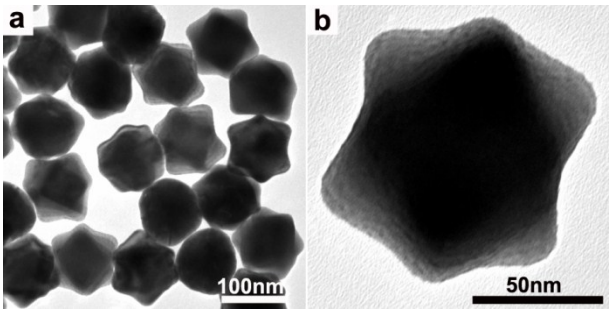

Figure S7. The digital photos of the aqueous solutions of TOH Au NPs, CS $Au_{100}@Pt_{20}$ NPs, and HTCS $Au_{100}@Pd_{20}Pt_{20}$ NPs, respectively.

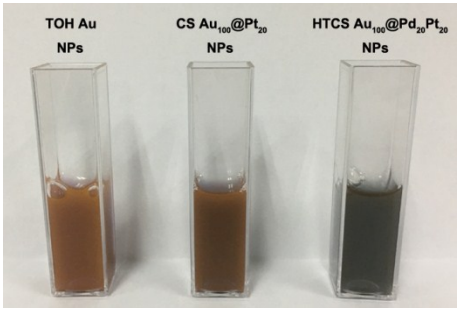

Figure S8. CV curves (A) and (B) of the GCE modified by $Au_{100}@Pt_{20}$ (a, black curve) and HTCS $Au_{100}@Pd_{20}Pt_{20}$ NPs (b, red curve), which were measured in 0.50 M H_2SO_4 solution in the absence (A) and presence (B) of 1.0 M methanol, respectively. The scan rates of (A) and (B) are 50 mV s^{-1} and 20 mV s^{-1}, respectively. The currents are normalized by the Pt mass loaded.

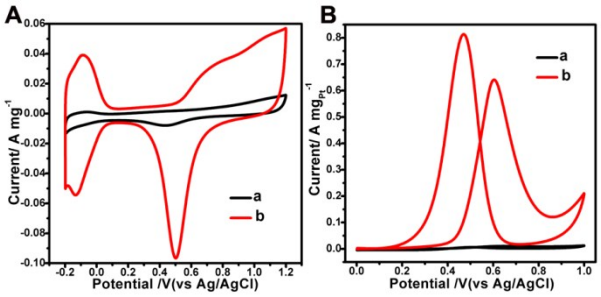

Figure S9. CV curves (A–C) of GCEs modified by HTCS $Au_{100}@Pd_{20}Pt_{20}$ NPs obtained at different AA-to-Pt molar ratios: 4 (a), 16 (b), 64 (c), 128 (d) and 256 (e), which were measured in 0.50 M H_2SO_4 solution in the absence (A) and presence (B and C) of 1.0 M methanol, respectively. The currents are normalized by the Pt mass loaded on the GCE (A and B) and ECSA values (C), respectively. The scan rates are 50 mV s^{-1} (A) and 20 mV s^{-1} (B and C), respectively.

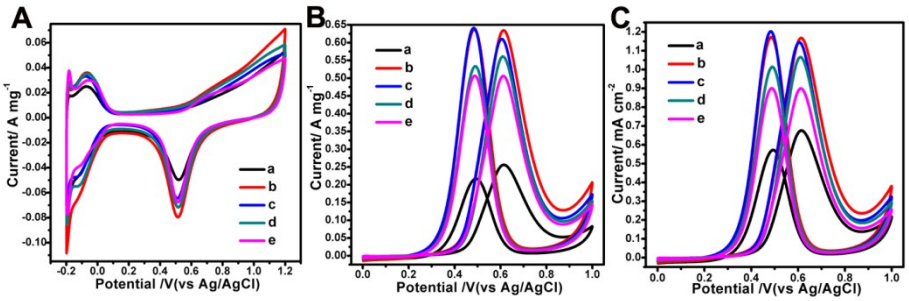

Figure S10. CV curves (A–C) of GCEs modified by HTCS Au@PdPt NPs obtained at different Pd-to-Pt molar ratios: 1.3:1 (a), 1.1:1 (b), 1:1 (c), 0.9:1 (d) and 0.8:1 (e), respectively, which were measured in 0.50 M H_2SO_4 solution in the absence (A) and presence (B and C) of 1.0 M methanol, respectively. The currents are normalized by the Pt mass loaded on the GCE (A and B) and ECSA values (C), respectively. The scan rates are 50 mV s^{-1} (A) and 20 mV s^{-1} (B and C), respectively.

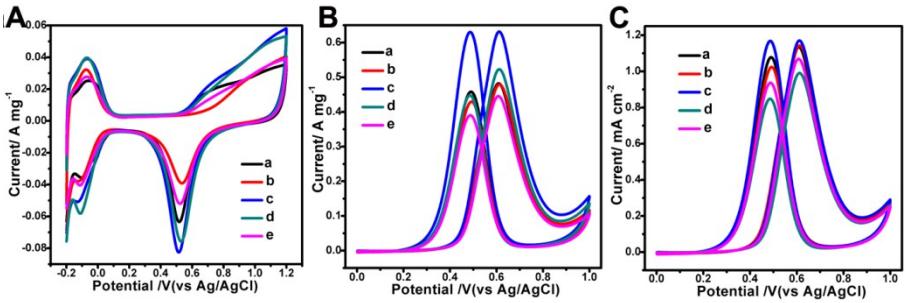

Figure S11. TEM images of HTCS $Au_{100}@Pd_{50}Pt_{50}$ (a), HTCS $Au_{100}@Pd_{25}Pt_{25}$ (b), HTCS $Au_{100}@Pd_{17}Pt_{17}$ (c), and HTCS $Au_{100}@Pd_{14}Pt_{14}$ NPs (d).

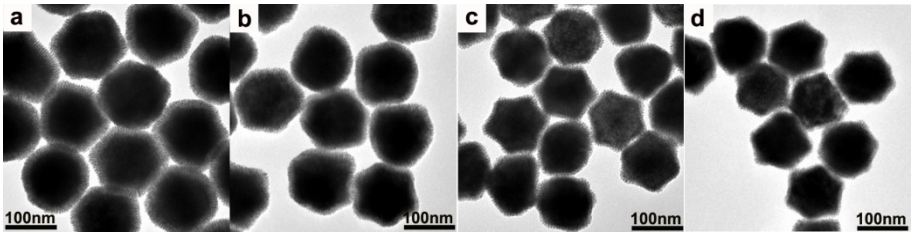

Figure S12. CV curves (A–C) of GCEs modified by HTCS $Au_{100}@Pd_{50}Pt_{50}$ NPs (a, black curve), $Au_{100}@Pd_{25}Pt_{25}$ NPs (b, red curve), $Au_{100}@Pd_{20}Pt_{20}$ NPs (c, blue curve), $Au_{100}@Pd_{17}Pt_{17}$ NPs (d, dark cyan curve), and $Au_{100}@Pd_{14}Pt_{14}$ NPs (e, magenta curve) measured in 0.50 M H_2SO_4 solution in the absence (A) and presence (B and C) of 1.0 M methanol. The currents are normalized by the Pt mass loaded on the GCE (A and B) and ECSA values (C), respectively. The scan rates are 50 mV s^{-1} (A) and 20 mV s^{-1} (B and C), respectively.

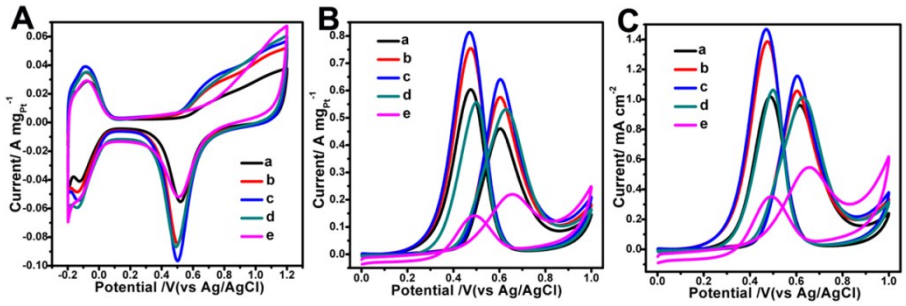

The ECSA values of HTCS $Au_{100}@Pd_{50}Pt_{50}$, $Au_{100}@Pd_{25}Pt_{25,}$ $Au_{100}@Pd_{20}Pt_{20}$, $Au_{100}@Pd_{17}Pt_{17}$, and $Au_{100}@Pd_{14}Pt_{14}$ NPs are calculated to be 42.34, 54.44, 55.42, 52.33, and 40.22 m^2 g^{-1} (Table S2), respectively, by measuring the charge collected in the hydrogen adsorption/ desorption region after double-layer correction in 0.5 M H_2SO_4 solution at room temperature at a scan rate of 50 mV s^{-1} (Figure S11A).

Figure S13. Low (a) and high magnification (b) TEM images of dendritic PdPt alloy NPs.

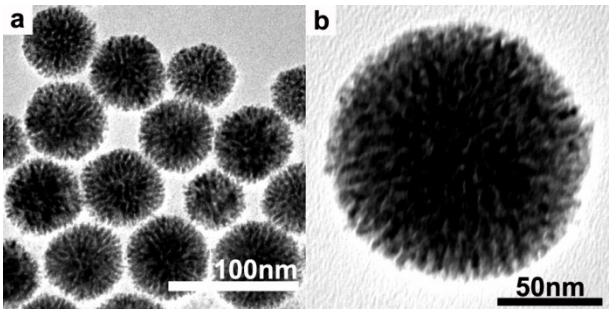

Typically, the aqueous solutions of Na_2PdCl_4 (25 mM, 100 μL), K_2PtCl_4 (25 mM, 100 μL) and AA (400 mM, 100 μL) were consecutively added into 5 mL of a 50 mM aqueous solution of CTAC, followed by gently shaking. The resultant solution was heated to 70℃ and maintained for 3h in the sealed vial. Eventually, dendritic PdPt alloy NPs were obtained. The aqueous dispersion of dendritic PdPt alloy NPs was subjected to centrifugation (6000 rpm for 5 min, three times) to remove excess reagents. Subsequently, the resulting dendritic PdPt alloy NPs were redispersed in water with the assistance of sonication to make a colloidal suspension for further characterization.

Figure S14. TEM images of spherical Au NPs (a) and HSCS $Au_{100}@Pd_{20}Pt_{20}$ NPs (b). The inset in (b) is the corresponding high magnification TEM images of HSCS $Au_{100}@Pd_{20}Pt_{20}$ NPs.

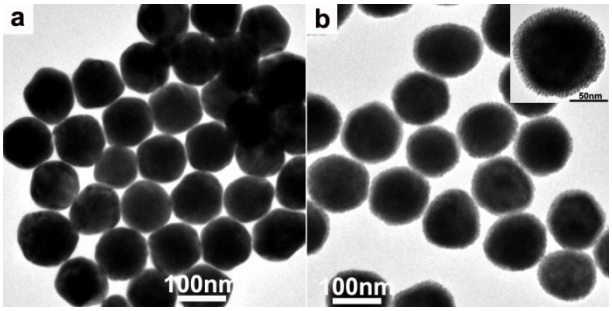

Figure S15. TEM images of octahedral Au NPs (a) and HOCS $Au_{100}@Pd_{20}Pt_{20}$ NPs (b). The inset in (b) is the corresponding high magnification TEM images of HOCS $Au_{100}@Pd_{20}Pt_{20}$ NPs.

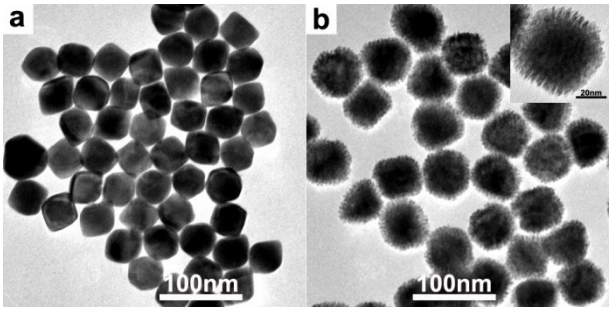

Figure S16. CV curves (A and B) and CA curves (C) of the GCEs modified by commercial Pt black (a, black curve), dendritic PdPt alloy NPs (b, red curve), HSCS $Au_{100}@Pd_{20}Pt_{20}$ NPs (c, blue curve), HOCS $Au_{100}@Pd_{20}Pt_{20}$ NPs (d, dark cyan curve), and HTCS $Au_{100}@Pd_{20}Pt_{20}$ NPs (e, magenta curve), respectively, which were measured in 0.50 M H_2SO_4 in the presence of 0.5 M formic acid. The currents were normalized by the Pt mass loaded on the GCE (A and C) and ECSA values (B), respectively. The scan rates (A and B) were 20 mV s^{-1}. CA curves (C) were recorded at 0.65 V.

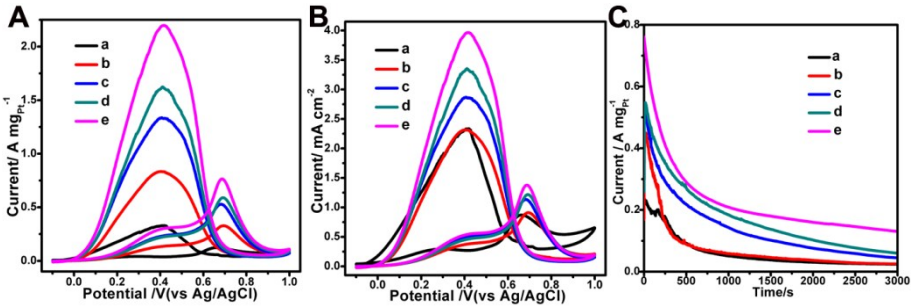

The electrochemical activities of the HTCS $Au_{100}@Pd_{20}Pt_{20}$ NPs on formic acid oxidation were also investigated. Figure S16A and B depict the mass and specific activities of the corresponding catalysts on formic acid oxidation recorded in 0.50 M H_2SO_4 solution in the presence 0.50 M formic acid at 20 mV s^{-1}. HTCS $Au_{100}@Pd_{20}Pt_{20}$ NPs exhibit a greatly improved mass-normalized current density (up to 0.77 A mg_{Pt}^{-1}), which is 6.42, 2.33, 1.48, and 1.33 times than that of commercial Pt black (0.12 A mg_{Pt}^{-1}), dendritic PdPt alloy NPs (0.33 A mg_{Pt}^{-1}), HSCS $Au_{100}@Pd_{20}Pt_{20}$ NPs (0.52 A mg_{Pt}^{-1}), and HOCS $Au_{100}@Pd_{20}Pt_{20}$ NPs (0.58 A mg_{Pt}^{-1}), respectively. Moreover, the HTCS $Au_{100}@Pd_{20}Pt_{20}$ NPs also exhibit a greatly improved specific activity (1.39 mA cm^{-2}) compared to that of other catalysts (Table S3), indicating that the defects (such as atomic steps, kinks, and corner atoms) on the surfaces of the PdPt nanobranches act as highly active sites for formic acid oxidation. In addition, CA curves for 3000 s also demonstrated the stability of HTCS $Au_{100}@Pd_{20}Pt_{20}$ NPs on the formic acid oxidation (Figure S16C). It is evident that the HTCS $Au_{100}@Pd_{20}Pt_{20}$ NPs also exhibit markedly enhanced electrocatalytic activity on formic acid oxidation among these catalysts.

Figure S17. Low (a) and high magnification (b) TEM image and HRTEM image (c) recorded from the boxed area of (b) of HTCS $Au_{100}@Pd_{20}Pt_{20}$ NPs collected after CA measurement.

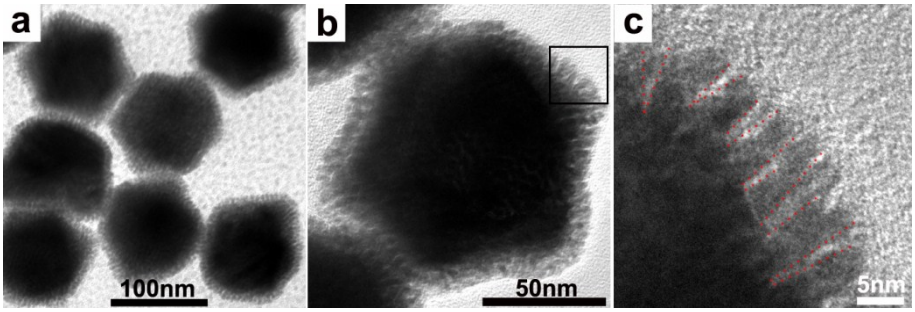

Figure S18. XPS spectra of the Pd 3d and Pt4d signals of dendritic PdPt alloy NPs (A) and HTCS $Au_{100}@Pd_{20}Pt_{20}$ NPs (B).

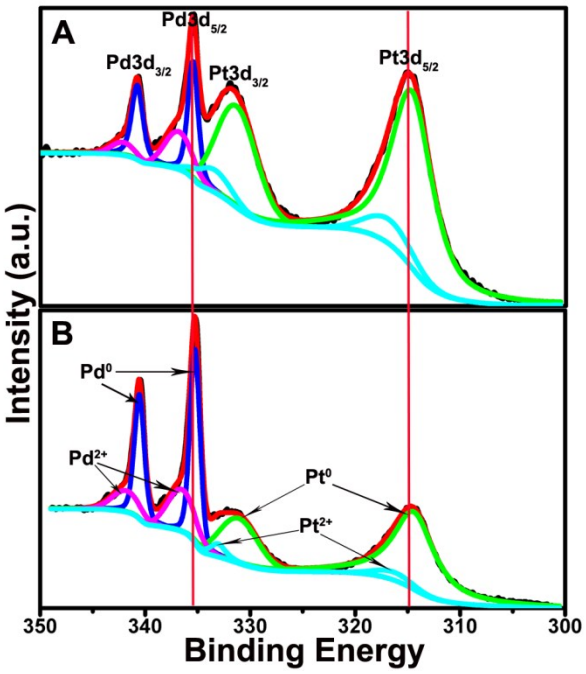

The peaks that appear at 340.0 and 335.0 eV in Figure S17 are assigned to Pd $3d_{3/2}$ and Pd $3d_{5/2}$, respectively.[1,2] Pd 3d could be deconvoluted into four individual peaks, i.e., 335.2 and 340.5 eV and 336.8 and 342.1 eV, corresponding to the metallic state (Pd^0) and oxide state (Pd^{2+}) of Pd, respectively. In addition, the BE values of Pd^0 $3d_{3/2}$ and Pd^0 $3d_{5/2}$ in the HTCS $Au_{100}@Pd_{20}Pt_{20}$ NPs also negatively shift ca. 0.3 eV compared to that of the dendritic PdPt alloy NPs (Table S4).

Figure S19. XPS spectra of the Au 4f signals of TOH Au NPs (A) and HTCS $Au_{100}@Pd_{20}Pt_{20}$ (B).

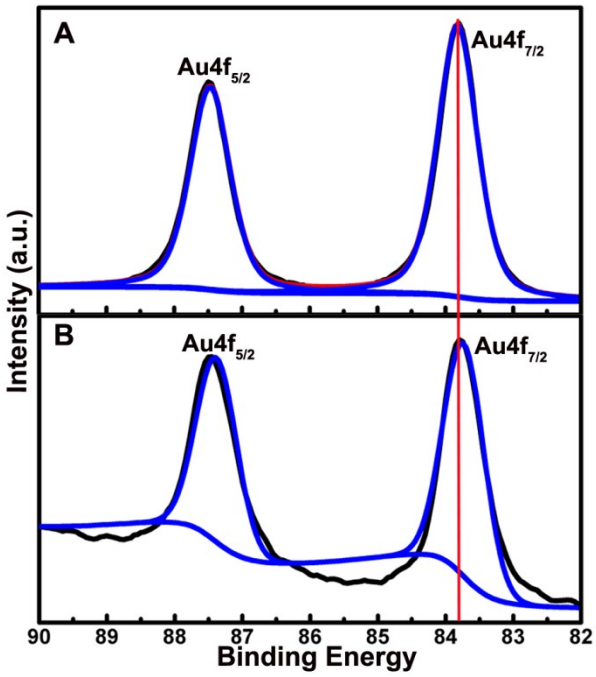

Figure S20. Representative SERS spectra of 4-ATP molecules (1×10^{-4} M) adsorbed on the aggregates of HTCS $Au_{100}@Pd_{20}Pt_{20}$ NPs, HOCS $Au_{100}@Pd_{20}Pt_{20}$ NPs, HSCS $Au_{100}@Pd_{20}Pt_{20}$ NPs, and dendritic PdPt alloy NPs on glass substrates. The excitation laser wavelength for Raman measurements is 633 nm. The acquisition time is 30 s.

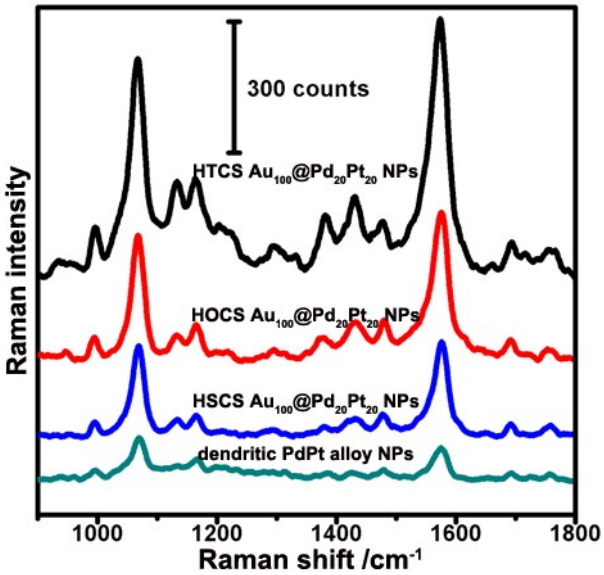

Figure S21. CO stripping measurements of commercial Pt black catalysts (a), commercial Pd/C catalysts (b), TOH Au NPs (c), dendritic PdPt alloy NPs (d) and HTCS $Au_{100}@Pd_{20}Pt_{20}$ NPs (e) performed in a solution of 0.50 M H_2SO_4 at 50 mV s^{-1}.

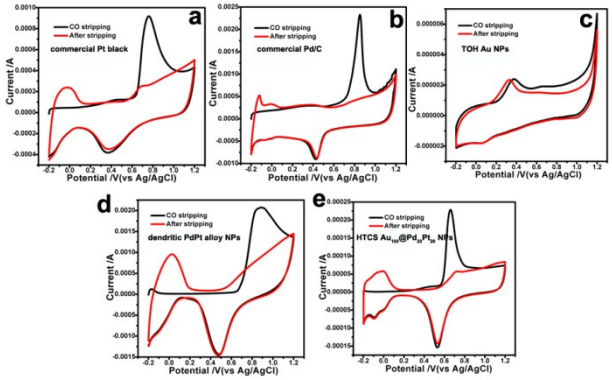

Table S1. Summary of the total compositions of TOH-shaped Au@Pd NPs and HTCS $Au_{100}@Pd_{20}Pt_{20}$ NPs by EDS.

Sample	Au(%)	Pd(%)	Pt(%)
TOH-shaped Au@Pd NPs	93.5	6.5	0
HTCS $Au_{100}@Pd_{20}Pt_{20}$ NPs	79.4	10	10.6

Table S2. Summary of molar ratio of Au/Pd/Pt, ECSAs, mass- and ECSA-normalized current densities of GCEs modified by HTCS $Au_{100}@Pd_{50}Pt_{50}$, $Au_{100}@Pd_{25}Pt_{25}$, $Au_{100}@Pd_{20}Pt_{20}$, $Au_{100}@Pd_{17}Pt_{17}$, and $Au_{100}@Pd_{14}Pt_{14}$ NPs as catalysts on methanol oxidation in 0.50 M H_2SO_4 solution containing 1.0 M methanol, respectively.

Sample	Molar ratio of Au/Pd/Pt	ECSA [$m^2\ g_{Pt}^{-1}$]	Mass activity [$A\ mg_{Pt}^{-1}$]	Specific activity [$mA\ cm^{-2}$]
HTCS $Au_{100}@Pd_{50}Pt_{50}$ NPs	1:0.5:0.5	42.34	0.41	0.92
HTCS $Au_{100}@Pd_{25}Pt_{25}$NPs	1:0.25:0.25	54.44	0.58	1.06
HTCS $Au_{100}@Pd_{20}Pt_{20}$ NPs	1:0.2:0.2	55.42	0.64	1.16
HTCS $Au_{100}@Pd_{17}Pt_{17}$ NPs	1:0.17:0.17	52.33	0.53	1.01
HTCS $Au_{100}@Pd_{14}Pt_{14}$ NPs	1:0.14:0.14	40.22	0.22	0.55

Table S3 Summary of the total compositions of HTCS $Au_{100}@Pd_{20}Pt_{20}$ NPs, HOCS $Au_{100}@Pd_{20}Pt_{20}$ NPs, and HSCS $Au_{100}@Pd_{20}Pt_{20}$ NPs by ICP-AES.

Sample	Au(%)	Pd(%)	Pt(%)
HTCS $Au_{100}@Pd_{20}Pt_{20}$ NPs	100	18.7	10
HOCS $Au_{100}@Pd_{20}Pt_{20}$ NPs	100	18.2	9.6
HSCS $Au_{100}@Pd_{20}Pt_{20}$ NPs	100	17.3	9.1

Table S4. Summary of mass- and ECSA-normalized current densities of GCEs modified by commercial Pt black, dendritic PdPt alloy NPs, HSCS $Au_{100}@Pd_{20}Pt_{20}$ NPs, HOCS $Au_{100}@Pd_{20}Pt_{20}$ NPs, and HTCS $Au_{100}@Pd_{20}Pt_{20}$ NPs as catalysts on formic acid oxidation in 0.50 M H_2SO_4 solution containing 0.50 M formic acid, respectively.

Sample	Mass activity [A mg_{Pt}^{-1}]	Specific activity [mA cm^{-2}]
commercial Pt black	0.12	0.86
dendritic PdPt alloy NPs	0.33	0.92
HSCS $Au_{100}@Pd_{20}Pt_{20}$ NPs	0.52	1.12
HOCS $Au_{100}@Pd_{20}Pt_{20}$ NPs	0.58	1.20
HTCS $Au_{100}@Pd_{20}Pt_{20}$ NPs	0.77	1.39

Table S5. XPS shifts for the Pd 3d signals for dendritic PdPt alloy NPs and HTCS $Au_{100}@Pd_{20}Pt_{20}$ NPs.

Sample	Pd $3d_{5/2}$ peak (eV)	Pd $3d_{3/2}$ peak (eV)	ΔPd $3d_{5/2}$ (eV)
dendritic PdPt alloy NPs	335.5	340.8	0
HTCS $Au_{100}@Pd_{20}Pt_{20}$NPs	335.2	340.5	-0.3

Table S6. XPS shifts for the Au 4f signals for TOH Au NPs and HTCS $Au_{100}@Pd_{20}Pt_{20}$ NPs.

Sample	Au $4f_{7/2}$ peak (eV)	Au $4f_{5/2}$ peak (eV)	ΔAu $4f_{7/2}$ (eV)
TOH Au NPs	83.8	87.45	0
HTCS $Au_{100}@Pd_{20}Pt_{20}$ NPs	83.76	87.41	-0.04

Reference

1. H. A. Esfahani, L. Wang, Y. Nemoto and Y. Yamauchi, *Chem. Mater.,* 2010, **22**, 6310.

2. Q. R. Shi, C. Z. Zhu, Y. J. Li, H. B. Xia, M. H. Engelhard, S. F. Fu, D. Du and Y. H. Lin, *Chem. Mater.,* 2016, **28**, 7928.